Lawrence Berkeley National Laboratory

Recent Work

Title

Tandem Catalysis for CO_2 Hydrogenation to C_2-C_4 Hydrocarbons.

Permalink

https://escholarship.org/uc/item/81k388rc

Journal

Nano letters, 17(6)

ISSN

1530-6984

Authors

Xie, Chenlu
Chen, Chen
Yu, Yi
et al.

Publication Date

2017-06-01

DOI

10.1021/acs.nanolett.7b01139

Peer reviewed

eScholarship.org Powered by the California Digital Library
University of California

NANO LETTERS

Letter

pubs.acs.org/NanoLett

Tandem Catalysis for CO_2 Hydrogenation to C_2−C_4 Hydrocarbons

Chenlu Xie,[†] Chen Chen,[†,∥] Yi Yu,[†,⊥] Ji Su,[‡] Yifan Li,[†] Gabor A. Somorjai,*[,†,‡] and Peidong Yang*[,†,‡,§]

[†]Department of Chemistry, University of California, Berkeley, California 94720, United States

[‡]Materials Sciences Division, Lawrence Berkeley National Laboratory, Berkeley, California 94720, United States

[§]Kavli Energy NanoScience Institute, Berkeley, California 94720, United States

Supporting Information

ABSTRACT: Conversion of carbon dioxide to C_2−C_4 hydrocarbons is a major pursuit in clean energy research. Despite tremendous efforts, the lack of well-defined catalysts in which the spatial arrangement of interfaces is precisely controlled hinders the development of more efficient catalysts and in-depth understanding of reaction mechanisms. Herein, we utilized the strategy of tandem catalysis to develop a well-defined nanostructured catalyst CeO_2−Pt@$mSiO_2$−Co for converting CO_2 to C_2−C_4 hydrocarbons using two metal-oxide interfaces. C_2−C_4 hydrocarbons are found to be produced with high (60%) selectivity, which is speculated to be the result of the two-step tandem process uniquely allowed by this catalyst. Namely, the Pt/CeO_2 interface converts CO_2 and H_2 to CO, and on the neighboring Co/$mSiO_2$ interface yields C_2−C_4 hydrocarbons through a subsequent Fischer−Tropsch process. In addition, the catalysts show no obvious deactivation over 40 h. The successful production of C_2−C_4 hydrocarbons via a tandem process on a rationally designed, structurally well-defined catalyst demonstrates the power of sophisticated structure control in designing nanostructured catalysts for multiple-step chemical conversions.

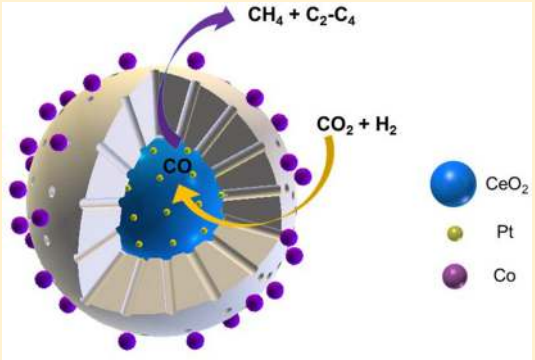

KEYWORDS: *CO_2 hydrogenation, tandem catalysis, interfaces, C_2−C_4 hydrocarbons*

Downloaded via UNIV OF CALIFORNIA BERKELEY on February 24, 2020 at 21:57:40 (UTC).
See https://pubs.acs.org/sharingguidelines for options on how to legitimately share published articles.

Transformation of CO_2 into transportable chemicals has been spurred by emerging environmental issues and rising energy demands.[1−5] Of particular interest is the synthesis of hydrocarbons containing two to four carbon atoms (C_2−C_4 hydrocarbons), which are key chemical feedstocks to synthesize a wide range of products such as polymers, solvents, drugs, and detergents. This is a challenging task because of the difficulties associated with the chemical inertness of CO_2 and the competing formation of methane.[6−8]

Currently, the conversion of CO_2 to C_2−C_4 hydrocarbons mainly relies on iron-based catalysts [via the Fischer−Tropsch process (F-T process)] and composite oxide catalysts such as Cu−ZnO−Al_2O_3/zeolite (via a methanol mediated pathway).[9−15] However, these catalysts are mostly synthesized through coprecipitation, impregnation, or physical mixing and contain multiple components including structural promoters. Thus, they exhibit large morphological variations and great uncertainties on the spatial arrangements of active sites.[10−12,16] We believe the development of structurally well-defined catalysts would not only facilitate discovery of new catalysts but also enable the fundamental study of reaction mechanisms to unravel principles for rational catalyst design. Specifically, the importance of spatial control of catalytic interfaces was emphasized in a recent development in tandem catalysis, where two metal-oxide interfaces in a single nanostructure were employed to catalyze two sequential chemical reactions.[17,18]

Herein, we demonstrate the rational design and controlled synthesis of a nanostructured catalyst with well-defined architecture for CO_2 conversion to C_2−C_4 hydrocarbons via tandem catalysis. The designed catalyst CeO_2−Pt@$mSiO_2$−Co ($mSiO_2$ denotes mesoporous silica) has two types of metal-oxide interfaces that catalyze two sequential reactions. The CeO_2/Pt interface converts CO_2 and H_2 into CO through the reverse water gas shift (RWGS) reaction, and the Co/$mSiO_2$ interface subsequently reacts the formed CO with H_2 through the Fischer−Tropsch process. Thus, this catalyst could carry out the CO_2 conversion to C_2−C_4 hydrocarbons through a two-step tandem process. As a result, a C_2−C_4 selectivity up to 60% of all hydrocarbons (carbon atom-based) through this tandem process was achieved.

To create these two interfaces, the catalyst was designed with a CeO_2−Pt core and a mesoporous silica shell, which is further decorated with cobalt nanoparticles. Considering the compatibility of synthetic conditions of different types of nanoparticles, the integration of all the four components in one single nanoparticle is challenging and requires an elegant synthetic design. In particular, synthesis of monodisperse cobalt nanoparticles could only be conducted under hydrophobic

Received: March 16, 2017
Revised: May 7, 2017
Published: May 11, 2017

© 2017 American Chemical Society

DOI: 10.1021/acs.nanolett.7b01139
Nano Lett. 2017, 17, 3798−3802

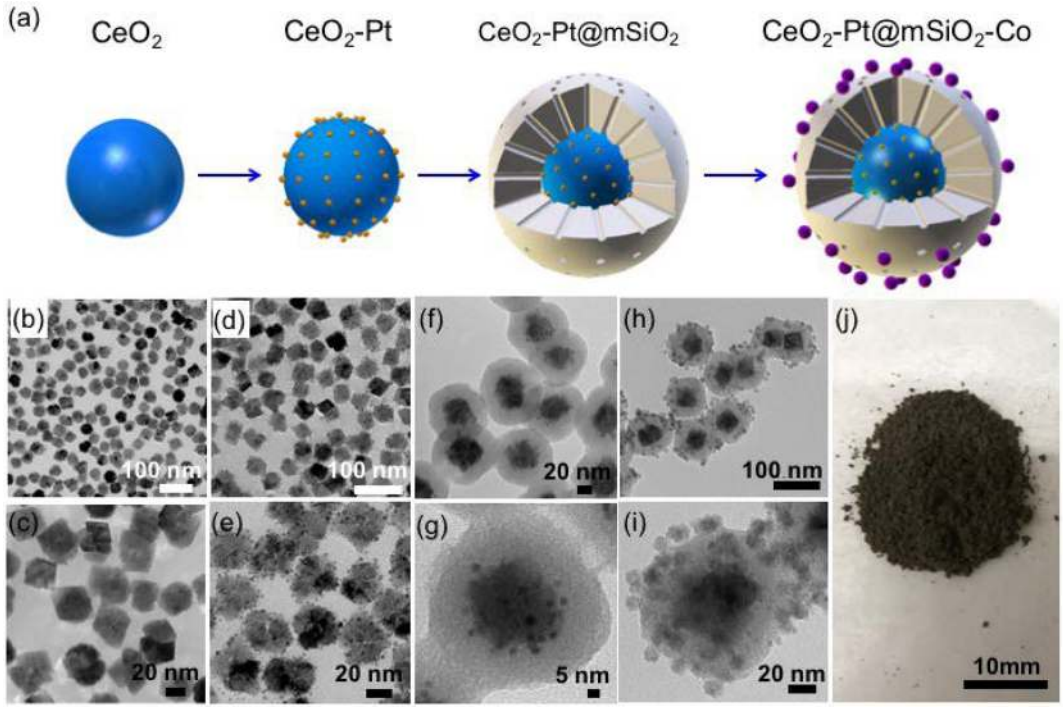

Figure 1. Synthesis and characterization of the CeO_2−Pt@$mSiO_2$−Co tandem catalyst. (a) Schematic of synthetic process. TEM images of each step: (b,c) CeO_2 nanoparticles, (d,e) overgrowth of Pt nanoparticles on CeO_2, (f,g) silica shell coating on CeO_2−Pt composite nanoparticles, (h,i) deposition of Co nanoparticles on CeO_2−Pt@$mSiO_2$, and (j) scaled up preparation of CeO_2−Pt@$mSiO_2$−Co nanoparticles. One-pot synthesis can yield 300 mg of catalyst.

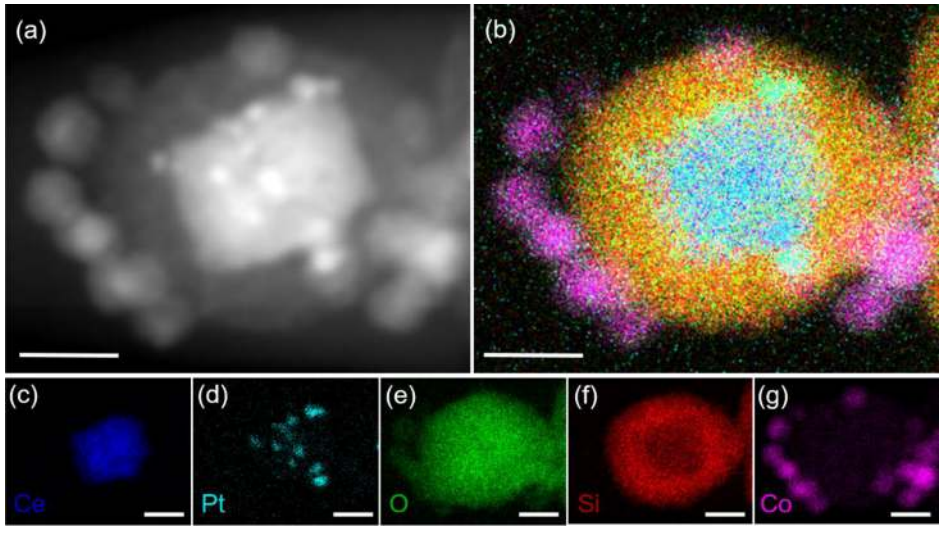

Figure 2. (a) Imaging of CeO_2−Pt@$mSiO_2$−Co by high-angle annular dark-field scanning transmission electron microscopy. (b) Elemental mapping of CeO_2−Pt@$mSiO_2$−Co with energy dispersive X-ray spectroscopy (EDS). Corresponding EDS elemental mapping for (c) Ce, (d) Pt, (e) O, (f) Si, and (g) Co, respectively. Scale bar: 20 nm.

conditions as they are prone to oxidation in aqueous solution, whereas the silica shell is typically synthesized in aqueous solution.[19−21] This incompatibility requires the preparation of monodisperse CeO_2−Pt@$mSiO_2$ and subsequent homogeneous loading of cobalt nanoparticles on the silica surface.

The optimized synthesis involves four steps. The first step is to synthesize well-dispersed and uniform CeO_2 nanoparticles. Considering that the subsequent silica coating step is typically performed in aqueous solution, the CeO_2 nanoparticles need to be dispersible in aqueous media. Thus, we carried out the synthesis of CeO_2 in ethanol and water solution with poly(vinylpyrrolidone) (PVP) as capping ligand.[18] This procedure enabled the production of uniform CeO_2 nanoparticles with very good dispersity, which is confirmed by transmission electron microscopy (TEM) (Figure 1b,c, Figure S1). The size of CeO_2 could be tuned by changing the ratio between ethanol and water. A higher ethanol/water ratio yields CeO_2 nanoparticles with smaller size (Figure S1). In order to gain higher dispersity of Pt nanoparticles on the CeO_2 support, a smaller CeO_2 nanoparticle with size around 35 nm was chosen. The second step is to load Pt nanoparticles onto the presynthesized CeO_2 nanoparticles by Pt overgrowth.[18,22]

DOI: 10.1021/acs.nanolett.7b01139
Nano Lett. 2017, 17, 3798−3802

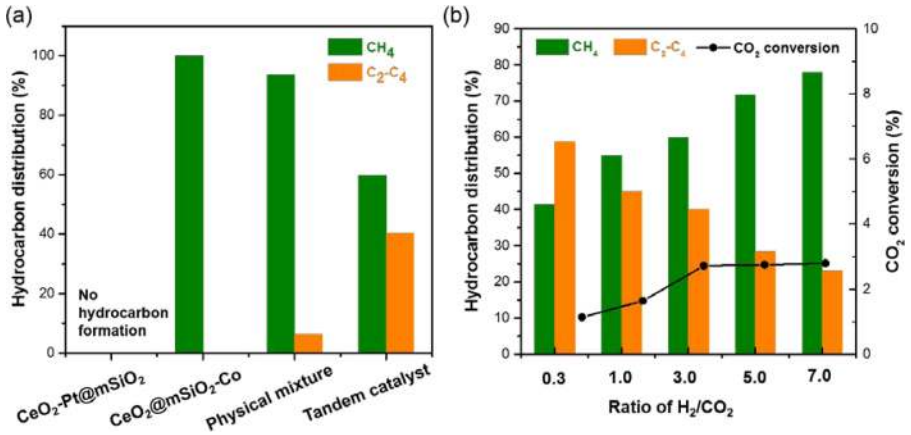

Figure 3. (a) Catalytic performance of single-interface catalysts CeO_2−Pt@$mSiO_2$ and CeO_2@$mSiO_2$−Co, physical mixture catalyst and tandem catalyst CeO_2−Pt@$mSiO_2$−Co (H_2/CO_2 ratio is 3, reaction temperature is 250 °C). (b) CO_2 conversion and hydrocarbons distribution at different H_2/CO_2 ratios over the tandem catalyst at 250 °C.

Tetradecyltrimethylammonium bromide (TTAB) and PVP were used as capping ligands to give 3 nm loaded Pt NPs (Figure 1d,e). Compared to the electrostatic absorption method, where the presynthesized Pt nanoparticles were absorbed on the CeO_2 surface, the overgrowth method gave stronger interaction between Pt and CeO_2, which helped maintain the structure of the nanocrystals in the silica coating step. Moreover, the loading amount of Pt could be easily tuned by adding different amount of $(NH_4)_2Pt(IV)Cl_6$ (Figure S2). Subsequently, a sol−gel approach was adopted to coat a mesoporous SiO_2 shell on the CeO_2−Pt core.[18,20,23,24] The as-synthesized CeO_2−Pt@SiO_2 was calcined at 350 °C in air to remove the cetrimonium bromide (CTAB) template to generate the mesopores and clean interfaces. The average thickness of the silica layer surrounding the CeO_2−Pt core was 25 nm (Figure 1f,g). With different amount of tetraethyl orthosilicate (TEOS) added, the thickness of the mesoporous silicon shell can be tuned (Figure S3). Finally, homogeneous loading of cobalt NPs on the silica shell was achieved by an approach utilizing the weak interactions between cobalt and silica in aprotic solvents.[25] Monodisperse Co nanoparticles were synthesized first by decomposing dicobalt carbonyl under the protection of oleic acid, which was dispersed in hexanes (Figure S4).[26] The as-synthesized CeO_2−Pt@$mSiO_2$ powder was also dispersed in hexanes, and the cobalt−hexanes solution was added slowly under stirring to gain a uniform distribution of cobalt nanoparticles on the silica shell. The dispersion of Co nanoparticles was then locked in place by calcination under air at 350 °C (Figure 1h,i), which simultaneously removed the oleic acid ligands.[25,27] This four-step synthesis of CeO_2−Pt@$mSiO_2$−Co can be readily scaled up to produce the tandem catalysts at gram scale (Figure 1j). This highly tunable and versatile synthetic protocol can be generalized toward the synthesis of other systems with multiple metal-oxide interfaces, which paves the way for the development of other sophisticated multifunctional catalysts for multistep chemical reactions.

High-angle annular dark-field scanning transmission electron microscopy (HAADF-STEM) and the corresponding energy-dispersive X-ray spectroscopy (EDS) mapping further confirmed the elemental distribution and structure of the catalyst (Figure 2). The Pt and Co loading were determined to be 4.3% and 5.8% (Table S1), respectively, from inductively coupled plasma atomic emission spectroscopy (ICP-AES). Nitrogen physisorption revealed the mesoporous nature of the catalyst, and its Brunauer−Emmett−Teller (BET) surface area was calculated to be 236 $m^2\ g^{-1}$ with average pore size of 2.4 nm, which provides accessibility to reactant molecules (Figure S5).

The catalytic performance of the tandem catalyst for CO_2 hydrogenation was examined under a series of temperatures with a pressure of 90 psi and a H_2/CO_2 ratio of 3. To monitor the role of each interface individually, we prepared single-interface catalysts CeO_2−Pt@$mSiO_2$ and CeO_2@$mSiO_2$−Co and tested their catalytic performance under the same conditions. Pt and Co loading amounts of these catalysts were controlled to be identical to the tandem catalyst (Table S1). It is known that Pt loaded on CeO_2 shows high activity and selectivity toward CO_2 hydrogenation to produce CO through the RWGS reaction,[28,29] while supported Co catalysts are widely used for hydrocarbons production from CO via the F-T process.[30−34] However, supported Co catalysts were reported to be almost only active for methane formation when replacing CO by CO_2 and a high CO partial pressure is necessary for the production of hydrocarbons beyond methane.[32,35−37] As shown in Figure 3a and Figure S6, the CeO_2−Pt@$mSiO_2$ catalyst indeed produced CO with excellent selectivity (>99%) at all temperatures, which substantiated that CO_2 and H_2 could be converted into CO via RWGS reaction on Pt/CeO_2 interface in the tandem catalyst. As to the CeO_2@$mSiO_2$−Co catalyst, CO_2 hydrogenation over the catalyst led to methane as the only hydrocarbon product at 250 °C (Figure 3a). With elevated temperatures, methane was still the dominant product with selectivity >99%, with a very small amount of C_2−C_4 hydrocarbon produced (Figure S7).

Upon controlled integration of Pt/CeO_2 interface and Co/$mSiO_2$ interface into a tandem catalyst, the products shifted and the formation of C_2−C_4 hydrocarbons was clearly observed with a selectivity of 40% whereas methane selectivity dropped to 60% at 250 °C (Figure 3a). At increased temperatures, the selectivity toward C_2−C_4 hydrocarbons decreased but was still well above the C_2−C_4 hydrocarbons production over the single-interface catalysts (Figures S6, S7, and S9). The decline in selectivity toward C_2−C_4 hydrocarbons under higher temperature is due to the more favorable methanation of CO at higher temperature.[38] This outstanding selectivity toward C_2−C_4, not observed for the single-interface catalysts, suggests that CO_2 hydrogenation to C_2−C_4 hydrocarbons on the CeO_2−Pt@$mSiO_2$−Co catalyst undergoes a tandem process. The uniqueness of the tandem catalyst is further confirmed by

DOI: 10.1021/acs.nanolett.7b01139
Nano Lett. 2017, 17, 3798−3802

the comparison with a physical mixture of $Pt-CeO_2$ and $Co-SiO_2$, which produced methane as a primary product and only a small amount of C_2-C_4 hydrocarbons at all temperatures (Figure 3a and Figure S8). As the Co catalysts produce mainly CH_4 from CO_2 and a high CO/CO_2 ratio is necessary for C_2-C_4 hydrocarbons formation,[32,35−37] we speculated that favorable formation of C_2-C_4 in the tandem system could be attributed to the locally high CO partial pressure at the $Co/mSiO_2$ interface due to the well-controlled spatial arrangement of Pt/CeO_2 and cobalt nanocrystals. Considering the well-defined core−shell structure and confinement of Pt/CeO_2 interface within the mesoporous silica shell, all produced CO molecules on Pt/CeO_2 interface can be transported to the neighboring cobalt surface before diffusing out of the shell. Moreover, CO molecules have shown a higher sticking probability to cobalt than CO_2 and could be strongly adsorbed on a cobalt surface.[39] Consequently, a CO-rich local environment at the $Co/mSiO_2$ interface was created, which favors the production of C_2-C_4 hydrocarbons. In the case of a physical mixture, however, the uncontrolled spatial arrangement of the $Pt-CeO_2$ and $Co-SiO_2$ interfaces resulted in a very low chance for CO from $Pt-CeO_2$ to be involved in the second reaction. Thus, the low CO partial pressure on the $Co/mSiO_2$ interface in the physical mixture catalysts resulted in low selectivity toward C_2-C_4 hydrocarbons. In accordance with our hypothesis, any measures that could further increase the localized CO partial pressure at Co/SiO_2 interface should benefit the selectivity of C_2-C_4 hydrocarbons, for example, decreasing the H_2/CO_2 ratio. This in turn would decrease the H_2/CO ratio for the second F-T reaction, and thus lead to a more localized CO environment in Co/SiO_2 interface. As demonstrated in Figure 3b, with the H_2/CO_2 ratio decreased from 7.0 to 0.3 the selectivity toward C_2-C_4 hydrocarbons increased from 23% to 59%, while the selectivity of methane dropped from 77% to 41%.

The harsh reaction conditions employed to study these reactions prompted us to examine the stability of the catalyst and its performance. As shown in Figure 4 and Figure S10, the

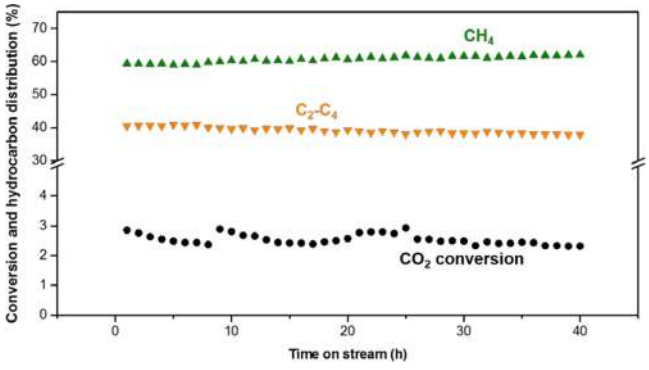

Figure 4. Stability test of $CeO_2-Pt@mSiO_2-Co$ catalyst with H_2/CO_2 of 3.0 at 250 °C.

$CeO_2-Pt@mSiO_2-Co$ tandem catalyst produced no significant change in catalytic activity and product selectivity while running the catalysts for up to 40 h. Moreover, the tested catalysts were also evaluated by TEM, and no obvious morphology change was observed (shown in Figure S11), indicating good structural and chemical stability of the tandem catalysts.

In conclusion, we developed a highly tunable method to synthesize a well-defined nanostructured catalyst $CeO_2-Pt@mSiO_2-Co$ for the selective production of C_2-C_4 hydrocarbons from CO_2. This catalyst achieved a selectivity of 60% toward C_2-C_4 hydrocarbons with two interfaces Pt/CeO_2 and Co/SiO_2 in close proximity, catalyzing the RWGS reaction and the F-T reaction, respectively. This high C_2-C_4 hydrocarbons selectivity is attributed to the unique spatial arrangement of two metal-oxide interfaces, which creates local environments conducive for multistep reactions that a physical mixture fails to achieve. Our synthetic protocol offers a highly generalizable method to integrate different metal-oxide interfaces for design and synthesis of next generation nanostructured catalysts. These advances give impetus to the rational design and development of high-performance, multifunctional catalysts for multiple-step chemical conversions.

■ ASSOCIATED CONTENT

Supporting Information

The Supporting Information is available free of charge on the ACS Publications website at DOI: 10.1021/acs.nanolett.7b01139.

Detailed protocol for nanoparticles synthesis and catalytic performance test, TEM images of catalysts with different size, loading amount and silica thickness and catalytic performance of catalysts under different temperatures (PDF)

■ AUTHOR INFORMATION

Corresponding Authors

*E-mail: somorjai@berkeley.edu (G.A.S.).
*E-mail: p_yang@berkeley.edu (P.Y.).

ORCID

Chenlu Xie: 0000-0001-9215-6878
Yifan Li: 0000-0003-2146-2266
Gabor A. Somorjai: 0000-0002-8478-2761
Peidong Yang: 0000-0003-4799-1684

Present Addresses

‖(C.C.) Department of Chemistry, Tsinghua University, Beijing 100084, P. R. China.
⊥(Y.Y.) School of Physical Science and Technology, ShanghaiTech University, Shanghai. 201210, China

Author Contributions

The manuscript was written through contributions of all authors. All authors have given approval to the final version of the manuscript. C.X., and C.C. contributed equally to this work.

Notes

The authors declare no competing financial interest.

■ ACKNOWLEDGMENTS

This work was supported by the U.S. Department of Energy, Office of Science, Office of Basic Energy Sciences (BES), Materials Sciences and Engineering Division, under Contract No. DE-AC02-05-CH11231 within the Chemical and Mechanical Properties of Surfaces, Interfaces and Nanostructures program (FWP KC3101). Work at the Molecular Foundry was supported by the U.S. Department of Energy, Office of Science, Office of Basic Energy Sciences under Contract No. DE-AC02-05-CH11231. This work made use of the facilities at the ICP facility, College of Chemistry, University of California, Berkeley. C.X. acknowledges support from Suzhou Industrial Park fellowship.

DOI: 10.1021/acs.nanolett.7b01139
Nano Lett. 2017, 17, 3798−3802

REFERENCES

(1) Dresselhaus, M. S.; Thomas, I. L. *Nature* **2001**, *414*, 332−337.
(2) Lewis, N. S.; Nocera, D. G. *Proc. Natl. Acad. Sci. U. S. A.* **2006**, *103*, 15729−15735.
(3) Aresta, M. Carbon Dioxide: Utilization Options to Reduce its Accumulation in the Atmosphere. *In Carbon Dioxide as Chemical Feedstock*; Wiley-VCH Verlag GmbH & Co. KGaA, 2010; pp 1−13.
(4) Graciani, J.; Mudiyanselage, K.; Xu, F.; Baber, A. E.; Evans, J.; Senanayake, S. D.; Stacchiola, D. J.; Liu, P.; Hrbek, J.; Sanz, J. F.; Rodriguez, J. A. *Science* **2014**, *345*, 546−550.
(5) Li, C.-S.; Melaet, G.; Ralston, W. T.; An, K.; Brooks, C.; Ye, Y.; Liu, Y.-S.; Zhu, J.; Guo, J.; Alayoglu, S.; Somorjai, G. A. *Nat. Commun.* **2015**, *6*, 6538.
(6) Rodemerck, U.; Holeňa, M.; Wagner, E.; Smejkal, Q.; Barkschat, A.; Baerns, M. *ChemCatChem* **2013**, *5*, 1948−1955.
(7) Müller, K.; Mokrushina, L.; Arlt, W. *Chem. Ing. Tech.* **2014**, *86*, 497−503.
(8) Dorner, R. W.; Hardy, D. R.; Williams, F. W.; Willauer, H. D. *Energy Environ. Sci.* **2010**, *3*, 884−890.
(9) Sai Prasad, P. S.; Bae, J. W.; Jun, K.-W.; Lee, K.-W. *Catal. Surv. Asia* **2008**, *12*, 170−183.
(10) Dorner, R. W.; Hardy, D. R.; Williams, F. W.; Willauer, H. D. *Appl. Catal., A* **2010**, *373*, 112−121.
(11) Kishan, G.; Lee, M.-W.; Nam, S.-S.; Choi, M.-J.; Lee, K.-W. *Catal. Lett.* **1998**, *56*, 215−219.
(12) Fujiwara, M.; Kieffer, R.; Ando, H.; Souma, Y. *Appl. Catal., A* **1995**, *121*, 113−124.
(13) Jeon, J.-K.; Jeong, K.-E.; Park, Y.-K.; Ihm, S.-K. *Appl. Catal., A* **1995**, *124*, 91−106.
(14) Satthawong, R.; Koizumi, N.; Song, C.; Prasassarakich, P. *Catal. Today* **2015**, *251*, 34−40.
(15) Niemelä, M.; Nokkosmäki, M. *Catal. Today* **2005**, *100*, 269−274.
(16) Riedel, T.; Schulz, H.; Schaub, G.; Jun, K.-W.; Hwang, J.-S.; Lee, K.-W. *Top. Catal.* **2003**, *26*, 41−54.
(17) Yamada, Y.; Tsung, C.-K.; Huang, W.; Huo, Z.; Habas, S. E.; Soejima, T.; Aliaga, C. E.; Somorjai, G. A.; Yang, P. *Nat. Chem.* **2011**, *3*, 372−376.
(18) Su, J.; Xie, C.; Chen, C.; Yu, Y.; Kennedy, G.; Somorjai, G. A.; Yang, P. *J. Am. Chem. Soc.* **2016**, *138*, 11568−11574.
(19) Kresge, C. T.; Leonowicz, M. E.; Roth, W. J.; Vartuli, J. C.; Beck, J. S. *Nature* **1992**, *359*, 710−712.
(20) Joo, S. H.; Park, J. Y.; Tsung, C.-K.; Yamada, Y.; Yang, P.; Somorjai, G. A. *Nat. Mater.* **2009**, *8*, 126−131.
(21) Qi, Z.; Xiao, C.; Liu, C.; Goh, T. W.; Zhou, L.; Maligal-Ganesh, R.; Pei, Y.; Li, X.; Curtiss, L. A.; Huang, W. *J. Am. Chem. Soc.* **2017**, *139*, 4762−4768.
(22) Tsung, C.-K.; Kuhn, J. N.; Huang, W.; Aliaga, C.; Hung, L.-I.; Somorjai, G. A.; Yang, P. *J. Am. Chem. Soc.* **2009**, *131*, 5816−5822.
(23) Zhao, E. W.; Maligal-Ganesh, R.; Xiao, C.; Goh, T.-W.; Qi, Z.; Pei, Y.; Hagelin-Weaver, H. E.; Huang, W.; Bowers, C. R. *Angew. Chem., Int. Ed.* **2017**, *56*, 3925−3929.
(24) Maligal-Ganesh, R. V.; Xiao, C.; Goh, T. W.; Wang, L.-L.; Gustafson, J.; Pei, Y.; Qi, Z.; Johnson, D. D.; Zhang, S.; Tao, F.; Huang, W. *ACS Catal.* **2016**, *6*, 1754−1763.
(25) Zheng, N.; Stucky, G. D. *J. Am. Chem. Soc.* **2006**, *128*, 14278−14280.
(26) Iablokov, V.; Beaumont, S. K.; Alayoglu, S.; Pushkarev, V. V.; Specht, C.; Gao, J.; Alivisatos, A. P.; Kruse, N.; Somorjai, G. A. *Nano Lett.* **2012**, *12*, 3091−3096.
(27) Ma, G.; Binder, A.; Chi, M.; Liu, C.; Jin, R.; Jiang, D.-e.; Fan, J.; Dai, S. *Chem. Commun.* **2012**, *48*, 11413−11415.
(28) Fu, Q.; Saltsburg, H.; Flytzani-Stephanopoulos, M. *Science* **2003**, *301*, 935−938.
(29) Goguet, A.; Meunier, F. C.; Tibiletti, D.; Breen, J. P.; Burch, R. *J. Phys. Chem. B* **2004**, *108*, 20240−20246.
(30) Iglesia, E. *Appl. Catal., A* **1997**, *161*, 59−78.
(31) den Breejen, J. P.; Radstake, P. B.; Bezemer, G. L.; Bitter, J. H.; Frøseth, V.; Holmen, A.; Jong, K. P. d. *J. Am. Chem. Soc.* **2009**, *131*, 7197−7203.
(32) Melaet, G.; Ralston, W. T.; Li, C.-S.; Alayoglu, S.; An, K.; Musselwhite, N.; Kalkan, B.; Somorjai, G. A. *J. Am. Chem. Soc.* **2014**, *136*, 2260−2263.
(33) Jacobs, G.; Das, T. K.; Zhang, Y.; Li, J.; Racoillet, G.; Davis, B. H. *Appl. Catal., A* **2002**, *233*, 263−281.
(34) Khodakov, A. Y.; Chu, W.; Fongarland, P. *Chem. Rev.* **2007**, *107*, 1692−1744.
(35) Riedel, T.; Claeys, M.; Schulz, H.; Schaub, G.; Nam, S.-S.; Jun, K.-W.; Choi, M.-J.; Kishan, G.; Lee, K.-W. *Appl. Catal., A* **1999**, *186*, 201−213.
(36) Zhang, Y.; Jacobs, G.; Sparks, D. E.; Dry, M. E.; Davis, B. H. *Catal. Today* **2002**, *71*, 411−418.
(37) Akin, A. N.; Ataman, M.; Aksoylu, A. E.; Önsan, Z. I. *React. Kinet. Catal. Lett.* **2002**, *76*, 265−270.
(38) Dry, M. E. *Catal. Today* **2002**, *71*, 227−241.
(39) Visconti, C. G.; Lietti, L.; Tronconi, E.; Forzatti, P.; Zennaro, R.; Finocchio, E. *Appl. Catal., A* **2009**, *355*, 61−68.

DOI: 10.1021/acs.nanolett.7b01139
Nano Lett. 2017, 17, 3798−3802